Chapter 4
Review of Numerical Methods of Solution

In this chapter we will discuss the numerical approaches to the moving load problem given in the literature. Most of them concern beam deflection. Unfortunately, comparison with exact analytical or semi-analytical results are rarely given. In most cases the authors compare their results with curves published by other researchers. The authors compute examples using different data and boundary conditions. They usually emphasize the agreement of their results with other computational methods. Unfortunately, results which coincide with an approximate method are not necessarily accurate as well. We should relate the results to analytical solutions or at least to solutions which fulfill the governing differential equations with possibly the lowest error. In this chapter we will compare the curves presented in these publications with semi-analytical results.

First we will consider a string, although this type of a structure is not frequently studied in the literature. Then we will describe the Bernoulli–Euler beam and the Timoshenko beam. The approaches in the literature deal with a moving non-inertial force and an inertial force. Some of them are devoted to a system with a point load or a distributed load.

Some published papers, even ones extensively cited by other authors, do not give an objective measure of the error. The authors claim that a slight visual coincidence with other curves proves its correctness. Moreover, they expect that differences in the results justify the advantages of the published approach and should convince one of its correctness.

First of all, we must warn against using an ad-hoc inertia lumping in neighbouring nodes of the mesh. The mass distribution proportional to the distances to the nodal points fails, and the results can not be accepted. In the case of a beam we are dealing with a parabolic differential equation in space. This fact results in smooth and infinitely fast bending of the entire structure. The local deformation is strongly influenced by other parts of the beam. The influence of a concentrated load of a different type is lower than in the case of a string or a membrane.

The development of computer methods has led to a series of works on numerical calculations, especially using the finite element method (FEM). This method is much more comprehensive than the analytical or semi-analytical methods. Papers

C.I. Bajer and B. Dyniewicz: Numerical Analysis of Vibrations of Structures, LNACM 65, pp. 77–93.
springerlink.com

discussing moving loads with constant or periodic amplitude [91, 145] are simple and rely on modifying the vector on the right hand side, step by step. The resulting work is presented in papers devoted to modelling the motion of a vehicle as a group of oscillators [37, 65, 89, 92, 135]. These problems require the coincidence of the displacements and forces of two subsystems: the main structure and the moving oscillator. For balancing the respective quantities in both systems a simple iterative procedure is applied. This method also involves a modification of the right-hand side vector. At the first stage the structure is loaded by dynamic forces at the contact points corresponding with the oscillators. As a result, the nodal displacements of a discrete structure are obtained. This allows us to determine the vertical displacement of a beam or a plate at the contact points with the oscillators. Displacements assumed as boundary conditions force the motion of the oscillator. This iterative procedure results in force–displacement equilibrium in a single time step. Unfortunately, the convergence of such a scheme is limited to a certain range of parameters, such as the travelling velocity, stiffness of the structure, inertia, and especially—the time step. Otherwise the iterative procedure must be more complex and time consuming.

The insertion of the inertia of the moving load effect requires not only a modification of the right-hand side vector, but also selected parts of the global inertia, damping, and stiffness matrices of the system, in every time step. The first study discussing the influence of the inertia of the moving mass was reported in [150]. An inertial load moving at a constant speed on the Euler beam was considered. Further works [38, 52, 120] are also related to beams or plates in which the nodal displacements and angles are interpolated by cubic polynomials. In these papers the derived matrices are not general. They are not suitable for use for the string or Timoshenko beam in which the nodal displacements and angles are interpolated by a linear function independently. In the literature, you can also find examples of the discrete element method for moving loads [100, 149]. This consists of replacing a beam by a system of rigid rods, connected among themselves on the basis of the compatibility of the rotation of adjacent elements.

The acceleration of a mass particle in the space-time domain is described by the Renaudot formula [118]. The different parts of the equation describe the lateral acceleration, Coriolis acceleration and centrifugal acceleration. The interpolation of the nodal displacements by a third order polynomial allows us to derive the matrices responsible for the travelling mass particle. Unfortunately, the Euler beam equation is not a wave equation. The study of a wave phenomena is possible by using a more complex model of the Timoshenko beam in which the vibration equation takes into account the influence of lateral forces and rotatory inertia on the deflection line of the beam. The angle formed by the axis of the deformed beam is composed of the pure bending angle and the angle corresponding to the deformation of the pure shear. Independent interpolation of displacements and rotation angles of the Timoshenko beam causes serious problems. Linear interpolation of nodal shape features renders impossible the designation of the centrifugal acceleration of a moving mass particle. In the previous works [24, 25, 26], we presented a method for determining the matrices responsible for the description of the moving mass by the space-time finite

element method with the use of a linear interpolation. We developed unique finite elements carrying a moving mass particle. It was not yet the general solution for practitioners. In engineering practice real structures possess a characteristic critical speed (of the load) in a range of about 200 km/h (in the case of railway tracks) and this can vary depending on structural details and environmental conditions.

4.1 Oscillator

The main advantage of computations based on the idea of only the spring elements being in contact with the main structure is the simplicity of the algorithms involved. Let us discuss the main features of this method.

First of all we can avoid the need to include the matrices resulting from time derivation of the displacement in the follower point. Incorporation of such matrices may cause serious problems. The matrices corresponding to the transverse acceleration and centrifugal acceleration are symmetric. Unfortunately the matrix describing the Coriolis acceleration is unsymmetrical. This fact may complicate the procedure, especially if we intend to use existing code which was prepared for symmetric matrices. Moreover we can not decompose the system of equations by using the diagonal inertia matrix and explicit time integration procedure. The main advantage of the massless spring's being in contact with the structure are having constant matrices in the system of algebraic equations. The right hand side vector is modified. However, this modification must be performed in an iterative way at each time step and convergence in the case of a complex structure can be poor or even lost in some circumstances.

The use of the oscillator instead of a rigid contact of the mass with a structure simplifies the computer codes and allows of performing computations in two separate threads, which enables a simple mutual exchange of displacements and forces. An example of such computations is presented in Algorithm 1.

4.1.1 String Vibrations under a Moving Oscillator

The simplest way of modelling a moving inertial load is an oscillator placed at the travelling contact point. In the case of a sufficiently rigid spring, we can consider the system as mass placed at a point. Unfortunately, the rigidity can not be assumed to be arbitrarily high. A low value does not ensure sufficient accuracy, while high values do not assure convergence. The algorithm to solve this has two stages. In the first one, we compute the point contact force on the base of the displacements of both ends of the spring of the oscillator. Then the string is subjected to this force, proportionally distributed to two neighbouring nodal points. In the second stage, the string displacements are computed. The displacements of the two subjected points allow of interpolating the vertical displacement at the intermediate points of the contact with the oscillator. This displacement, in turn, is imposed on the oscillator and determines the nodal contact force. Iteratively, we can equilibrate the forces in the two separate systems: the string and the oscillator (Algorithm 1). The

Algorithm 1. Solution of one time step performed for two structures in contact with mutual exchange of information

- Define the initial state at $t = t_i$:
  - external load applied to oscillator (substructure A),
  - displacements of the main structure (substructure B),
  - boundary condition at the contact point (c) of the oscillator (A), obtained with the interpolation formula, based on displacements of the substructure (B),
- execute one step of the calculations of the motion of the oscillator,
- determine the reaction (R) at point (c) of the oscillator,
- distribute the action force ($-R$) at the contact point (c) among the neighbouring nodes in the mesh by using a simple interpolation formula,
- solve one step of the motion of the structure (B) subjected to the forces resulting from the action ($-R$),
- select transverse displacements of the structure (B) in nodes neighbouring to the contact point (c),
- interpolate the displacements at point (c) based on the selected displacements at the neighbouring nodes in the mesh of the structure (B),
- use these displacements as the boundary conditions imposed on the contact points (c) of the oscillator (A),
- modify the external load to which is subjected the oscillator (A), if required,
- repeat the loop starting from the second point of this table until convergence is achieved,
- go to the next time step t_{i+1} and return to the beginning of this table.

convergence of the iterations will allow us to proceed to the next time step. However, wise choice of the solution methods applied to both stages of time integration is essential. Below we will present the results of a simple test. A moving oscillator forces the string motion.

In the first approach, we use the central difference method for the time integration of the equation of motion of the oscillator and the Newmark method for the remaining part, i.e. the string. We write: m – mass of the oscillator, k – oscillator stiffness, y_c – forced contact displacement of the bottom point of the oscillator, equal to $y_i^{(2)}$, $y_i^{(j)}$ – the j^{th} component of the displacement vector at time t_i, ie. $y_i^{(1)}$ is the displacement of the point which is in contact and $y_i^{(2)}$ is the displacement of the free end of the spring of the oscillator. We use the following formula for the oscillator:

$$\mathbf{y}_{i+1} = \begin{Bmatrix} y_{i+1}^{(1)} \\ y_{i+1}^{(2)} \end{Bmatrix} = \begin{Bmatrix} q_0 h^2/m + (2 - kh^2/m) y_i^{(1)} + kh^2/m \cdot y_i^{(2)} - y_{i-1}^{(1)} \\ y_c \end{Bmatrix} . \quad (4.1)$$

The contact force q is proportional to the spring elongation

$$q = k\left(y_{i+1}^{(1)} - y_{i+1}^{(2)}\right) \quad . \tag{4.2}$$

Simulations allowed us to verify the iterative procedure and its efficiency. We have two ways to fit the displacements of a contact point of the oscillator with the respective points of the string or beam. The first one is direct coincidence of the displacements of both points. In the second approach, we compare the velocities and we expect that if the time sequences of the velocities of both contact points are equal, the resulting contact of the two bodies is ensured. Still the influence of the spring rigidity on results may be severe. We performed this test with the hypothesis of the agreement of the displacements. The spatial domain of the string was divided into 100 finite elements. Dimensionless data was assumed: $l = 1$, $N = 1$, $\rho A = 1$. An extremely short time step was used ($h = 10^{-6}$). With the velocity $\mathrm{v} = 0.1$, this requires a large number, 10^7, of time steps. The spring stiffness $k = 10^2 - 10^4$ was assumed. The stiffness $k = 10^4$ resulted in divergence for a longer time step, $h = 10^{-4}$. The results are depicted in Figure 4.1. The displacements are scaled by the maximum static deflection w_0. We must emphasize that both in the above case and in the next example, the computations were performed at the limit of stability and convergence because of the values of the time step and spring stiffness. We notice that the accepted set of both parameters, i.e. time step and spring stiffness, gives procedures which are in practice ineffective.

Figure 4.2 shows the displacements of both ends of the oscillator spring. The mutual displacements are proportional to the contact force. We see that the contact force oscillates and is influenced by the spatial partition of the structure.

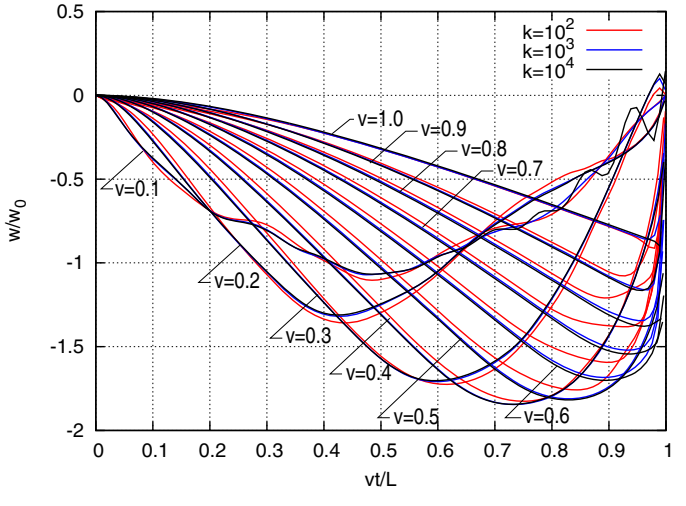

Fig. 4.1 Oscillator with $k = 10^2$, $k = 10^3$, and $k = 10^4$, moving on the string at various speeds.

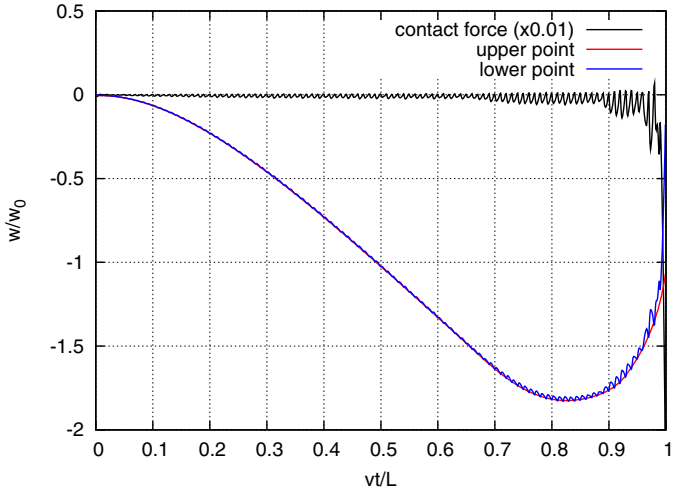

Fig. 4.2 Displacements of the upper and lower point of the spring of the oscillator at the speed $\mathrm{v} = 0.5\,c$, $k = 10^3$, $h = 10^{-5}$.

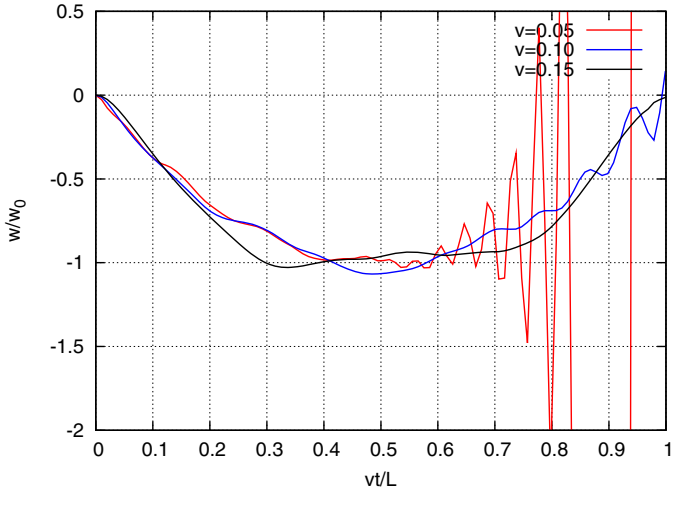

Fig. 4.3 Oscillator with $k = 10^4$, moving on the string at the speeds $\mathrm{v} = 0.05, 0.10$, and $0.15\,c$.

In the next approach, we apply the velocity formulas both to the oscillator and to the string. We assume that the equality of velocities of both substructures at the contact points ensures the equality of the displacements. The stages of the solution method are similar to the first case. Unfortunately, the convergence is unsatisfactory. First, we can not assume a sufficiently high rigidity of the spring. Decreasing the time step does not improve the situation. Neither can we complete the computations

for a higher velocity range. Figure 4.3 shows that sufficiently accurate results are obtained for the low speed of $\mathsf{v} \leq 0.1\,c$.

4.1.2 Beam Vibrations under a Moving Oscillator

Filho [52] considers a simple supported beam subjected to a moving oscillator composed of two masses: one supported with a Kelvin–Voigt spring–damper system m_1 and one placed at the contact point m_2 (Figure 4.4). The oscillator moves at a variable speed $\mathsf{v}(t)$ and constant horizontal acceleration a_0. The dynamic equilibrium equation of the mass m_1 is of the form

$$m_1\ddot{y} + c(\dot{y} - \dot{w}) + k(y - w) = 0 \quad . \tag{4.3}$$

The dynamic equilibrium of the mass m_2 and the structure was written in the matrix form

$$\mathbf{m}\ddot{\mathbf{d}} + \mathbf{c}\dot{\mathbf{d}} + \mathbf{k}\mathbf{d} = \mathbf{N}^T f_0 \quad . \tag{4.4}$$

In the above equations, **m**, **c**, and **k** are the inertia, damping, and stiffness matrices of the structure, respectively, **d** is the nodal displacement vector, and f_0 is the point load. The matrix **N** has zeros in all places except those corresponding to the degrees of freedom of the element with the positioned point force. **N** in fact is the interpolation matrix which distributes the point load between both element's nodes.

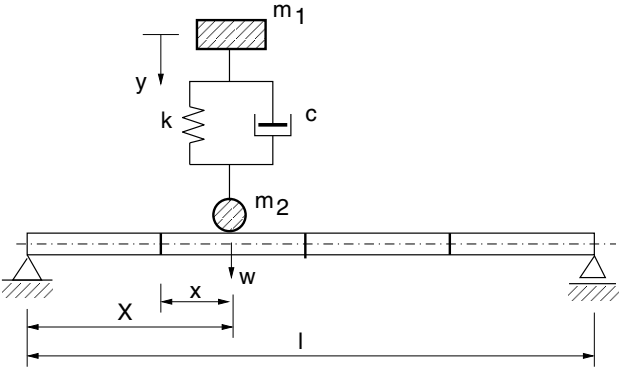

Fig. 4.4 Scheme of the discretized beam [52].

The force f_0 acting at the loaded element is composed of the gravity load of both masses, the inertial force of m_2, the damping force, and the spring force of the oscillator:

$$f_0 = (m_1 + m_2)g - m_2\ddot{w} + c(\dot{y} - \dot{w}) + k(y - w) \quad . \tag{4.5}$$

Here, the deflection w is determined at the moving contact point $x = \mathsf{v}t$. Its time derivatives are given by

$$\frac{\mathrm{d}w}{\mathrm{d}t} = \frac{\partial w}{\partial t} + \mathrm{v}\frac{\partial w}{\partial x}, \tag{4.6}$$

$$\frac{\mathrm{d}^2 w}{\mathrm{d}t^2} = \frac{\partial^2 w}{\partial t^2} + 2\mathrm{v}\frac{\partial^2 w}{\partial x \partial t} + \mathrm{v}^2\frac{\partial^2 w}{\partial x^2} + \frac{\mathrm{dv}}{\mathrm{d}t}\frac{\partial w}{\partial x}\ . \tag{4.7}$$

The deflection w is interpolated by nodal displacements

$$w(x,t) = \mathbf{N}(\mathbf{x})\mathbf{d}(t)\ . \tag{4.8}$$

The respective derivatives are computed

$$\frac{\partial^2 w}{\partial x^2} = \mathbf{N}''\mathbf{d},\ \ \frac{\partial^2 w}{\partial x \partial t} = \mathbf{N}'\dot{\mathbf{d}},\ \ \frac{\partial w}{\partial x} = \mathbf{N}'\mathbf{d},\ \ \frac{\partial^2 w}{\partial t^2} = \mathbf{N}\ddot{\mathbf{d}}\ , \tag{4.9}$$

and the distance is determined by integration $x = \mathrm{v}_0 t + a_0 t^2/2$. In such a case, $\dot{x} = \mathrm{v}_0 + a_0 t$ and $\ddot{x} = a_0$.

When we substitute the above formulas into (4.6) and (4.7), we obtain

$$\begin{aligned} \dot{w} &= (\mathrm{v}_0 + a_0 t)\mathbf{N}' + \mathbf{N}\dot{d}\ , \\ \ddot{w} &= (\mathrm{v}_0 + a_0 t)^2\mathbf{N}''\mathbf{d} + 2(\mathrm{v}_0 + a_0 t)\mathbf{N}'\dot{\mathbf{d}} + a_0\mathbf{N}'\mathbf{d} + \mathbf{N}\ddot{\mathbf{d}}\ . \end{aligned} \tag{4.10}$$

We put (4.10) into (4.8) and into the equilibrium equation (4.3). Finally we have

$$\begin{aligned} &\left[\begin{array}{c|c} \mathbf{M}+ & \\ +m_2\mathbf{N}^T\mathbf{N} & \mathbf{0} \\ \hline \mathbf{0}^T & m_1 \end{array}\right]\left\{\begin{array}{c}\ddot{\mathbf{d}}\\ \ddot{\mathbf{y}}\end{array}\right\} + \left[\begin{array}{c|c} \mathbf{C}+c\mathbf{N}^T\mathbf{N}+ & \\ +2m_2(\mathrm{v}_0+a_0t)\mathbf{N}^T\mathbf{N}' & -c\mathbf{N} \\ \hline -c\mathbf{N}^T & c \end{array}\right]\left\{\begin{array}{c}\dot{\mathbf{d}}\\ \dot{\mathbf{y}}\end{array}\right\} + \\ &+\left[\begin{array}{c|c} \mathbf{K}+m_2(\mathrm{v}_0t+a_0t^2)^2\mathbf{N}^T\mathbf{N}''+ & \\ +m_2a_0\mathbf{N}^T\mathbf{N}'+k\mathbf{N}^T\mathbf{N}+ & \\ +c(\mathrm{v}_0+a_0t)\mathbf{N}^T\mathbf{N}' & -k\mathbf{N}^T \\ \hline -c(\mathrm{v}_0+a_0t)\mathbf{N}'-k\mathbf{N} & k \end{array}\right]\left\{\begin{array}{c}\mathbf{d}\\ \mathbf{y}\end{array}\right\} = \left[\begin{array}{c}(m_1+m_2)g\mathbf{N}^T\\ \mathbf{0}\end{array}\right]\ . \end{aligned} \tag{4.11}$$

The matrix equation (4.11) is a linear equation with variable coefficients depending on t. In the particular case of $k = 0$, $c = 0$, and $f_0 = (m_1 + m_2)g$, we have a problem with a non-inertial force.

4.2 Inertial Load

In this section we will discuss numerical approaches to inertial loads given in the literature. Most of them concern beams. Unfortunately, in the literature, comparisons with exact analytical results are rarely given. In most cases, the authors compare their results with other published curves obtained from other approximate methods.

Let us look at the simple ad-hoc mass insertion: the mass is added proportionally to the distance from the element joints. Such a procedure can be performed by finite element analysis software if we can only push the load through the spatial element. A string vibration analysis enables plotting curves only in the case of a low string inertia and a low speed of the motion.

Plots for the inertial load in the case of the mass moving over the string differ from the analytical ones. Figure 4.5 shows the results at various speeds for the mass $m = 10$. Figure 4.6 presents the results for $m = 1$ and $\mathsf{v} = 0.1$, for $m = 1000$ and $\mathsf{v} = 0.2$, and for low values of both parameters: $m = 0.01$ and $\mathsf{v} = 0.1$. We notice that only in the case of low mass, i.e. almost a non-inertial load and at the low speed $\mathsf{v} = 0.1$ do we have agreement with the semi-analytical results.

4.2.1 A Bernoulli–Euler Beam Subjected to an Inertial Load

The solution procedure is relatively simple in the case of the Bernoulli–Euler beam with third order shape functions.

Consider Figure 4.7. Results in the literature [2] were compared with our results obtained with the space-time finite element method. The displacements of a free and of a cantilever beam subjected to a moving inertial point load are depicted. The velocity v of the moving load was equal to 0.27 of the critical speed $\mathsf{v}_{cr} = \pi/l \cdot \sqrt{EI/\rho/A}$. The following data was assumed: $l = 7.62$ m, $E = 20.68 \cdot 10^{10}$ Pa, $I = 4.58 \cdot 10^{-5}$ m^2, and $\mathsf{v} = 50.8$ m/s. Notice that the curve exhibiting the influence of the mass does not coincide with the numerical results (Figure 4.7a). On the other hand, the massless load in the same example has a perfect coincidence (Figure 4.7b).

Although Figure 4.7 was plotted for relatively high speed, other examples in the literature present results at low speeds around 0.01—0.05 of the wave speed. Unfortunately, in practice, we have a significantly higher ratio of the travelling velocity to the wave velocity. Such occurs in track dynamics, with a ballast that significantly increases the inertia and reduces the wave speeds. In such cases, the ratio can reach 0.1—0.5. Moreover, the existence of a point mass of a relatively high magnitude, compared with the beam mass, instead of a spring–mass system, increases the differences between the results obtained with the various methods at high speeds. That is why a simple, efficient, and accurate numerical tool is essential for engineering practice.

We next show results of numerical analyses of the Bernoulli–Euler beam taken from the literature. We have taken data from Sadiku [122] and Stanisic [128]. They are as follows: $l = 6$ m, $\mathsf{v} = 6$ m/s, $EI/\rho/A = 275.4408$ m^4/s^2, $m/\rho/A/l$=0.2, $g = 9.81$ m/s^2.

We present a plot with displacements under a mass moving along a simply supported Bernoulli–Euler beam (Figure 4.8). The results given by Stanisic practically coincide with the precise finite element solution. The data for creating the figure was taken from a digitalized article's plot and may not be accurate. This could explain the slight differences visible between both curves.

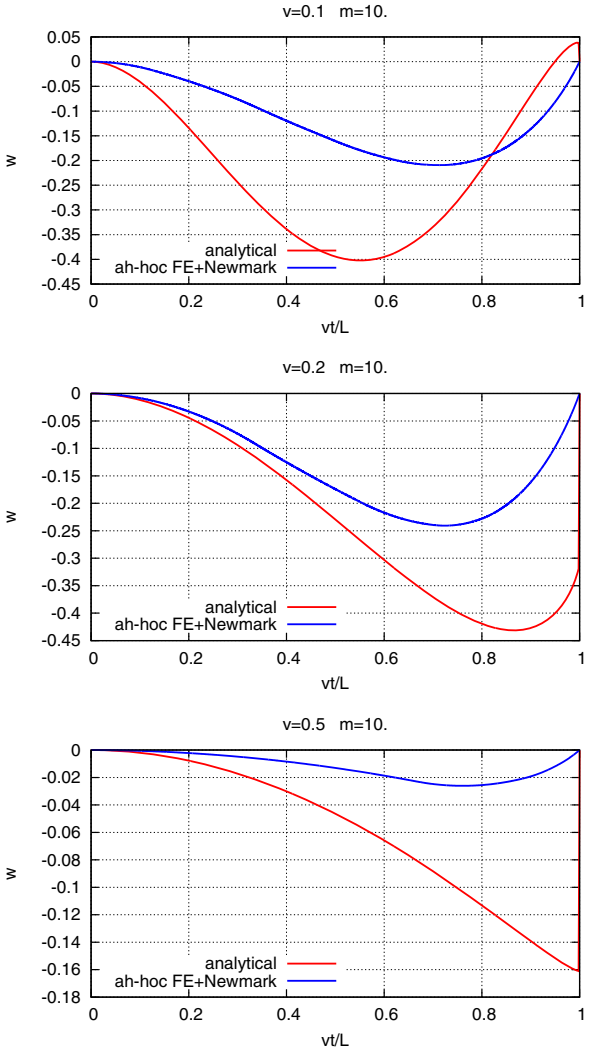

Fig. 4.5 Comparison of the ad-hoc finite element solution with semi-analytical results for a ratio of the moving mass to the string mass equal to 10, and at velocities $0.1c$, $0.2c$, and $0.5c$ ($c = 1$).

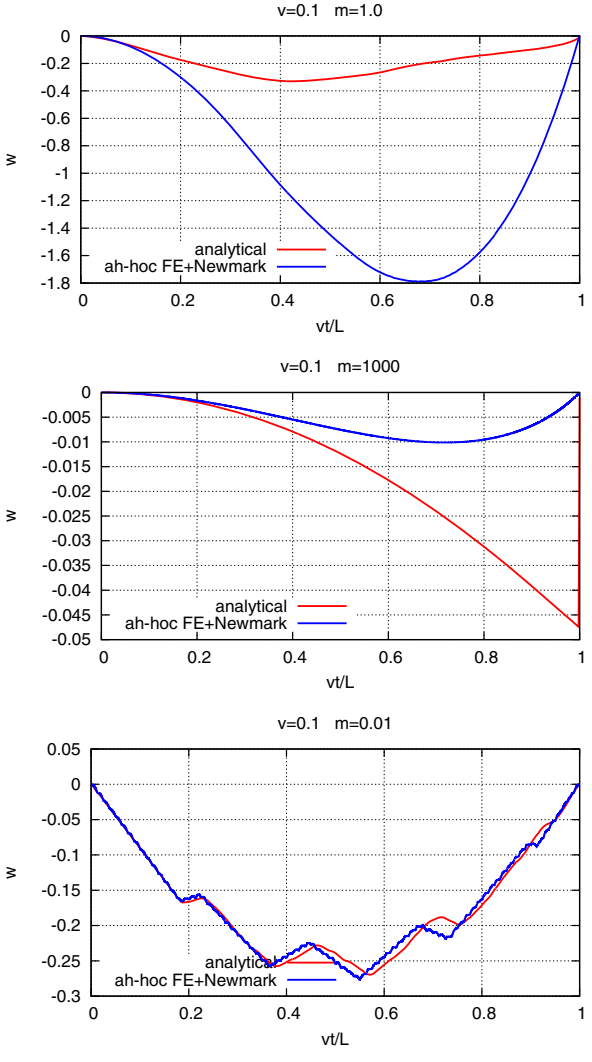

Fig. 4.6 Comparison of the ad-hoc finite element solution with semi-analytical results at various masses and velocities in the case of a string.

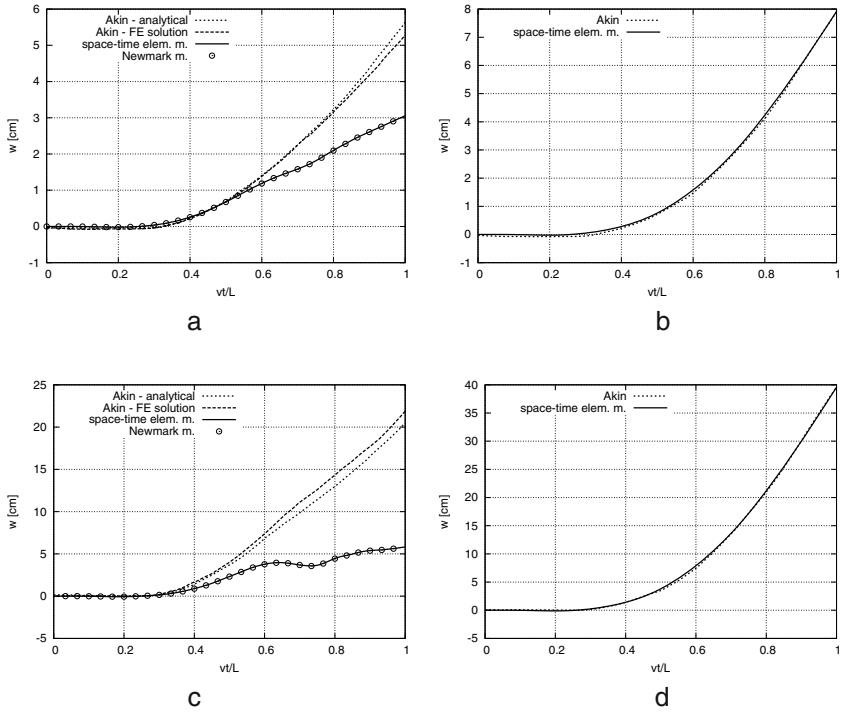

Fig. 4.7 Deflection at the end point of a Bernoulli–Euler cantilever beam subjected to (a) an inertial and (b) a non-inertial load for mass $m = 525.35$ kg and, respectively, (c) and (d) for $m = 2626.75$ kg [2].

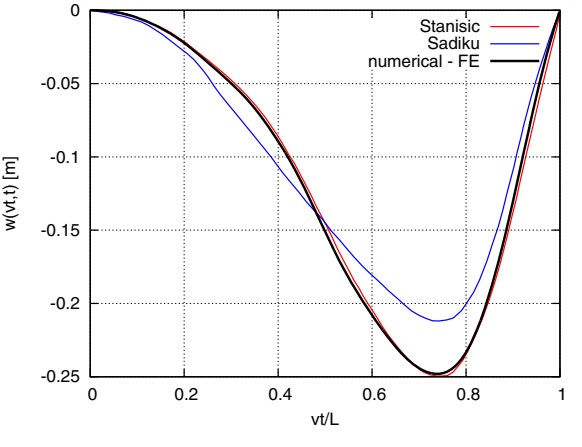

Fig. 4.8 Deflection under the moving mass.

The same data was used in Lee [85]. The clamped–clamped beam has been solved. Also, these results were assumed for comparison (Figures 4.9 and 4.10).

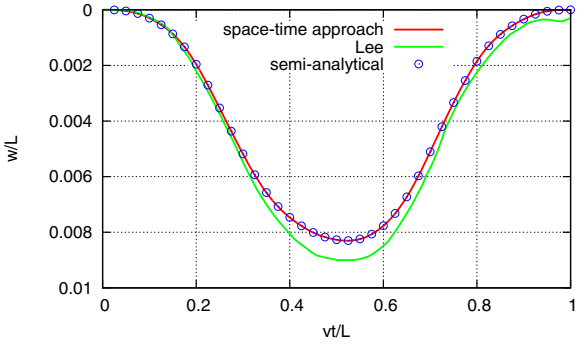

Fig. 4.9 The dimensionless deflection under a moving load for a clamped–clamped Euler beam at speed 0.5v.

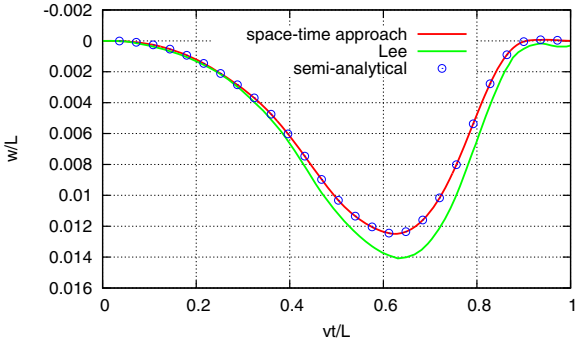

Fig. 4.10 The dimensionless deflection under a moving load for a clamped–clamped Euler beam at speed 1.2v.

In further chapters we will see that a correct derivation of the term describing the displacement of the moving point is essential. These results differ and do not coincide with the analytical results. What is more, the analytical curves given in the literature are also doubtful. In this book we will show both the correct analytical or semi-analytical and numerical solutions which coincide precisely with them.

4.2.2 A Timoshenko Beam Subjected to an Inertial Load

Mackertish in [95] presents the dynamic response of a simply supported Timoshenko beam excited by a moving mass that moves at a constant speed. The solution was obtained analytically and then the final results were computed numerically. The shear deformation and rotatory inertia effects were included.

The following data were assumed: $l = 50$ m, $\rho = 2400$ kg/m^3, $E = 3.36 \cdot 10^{10}$ Pa, $G = 1.40 \cdot 10^{10}$ Pa, $A = 2$ m^2, $I = 1.042$ m^4, and the shape factor $k = 1.2$. The moving mass m_0 =50,000 kg was moving with speeds v = 25 m/s, 50 m/s, and

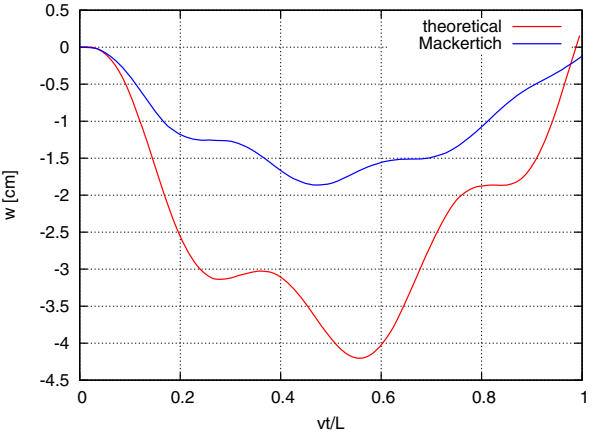

Fig. 4.11 Comparison of results given in [95] with semi-analytical results at the speed v = 25 m/s.

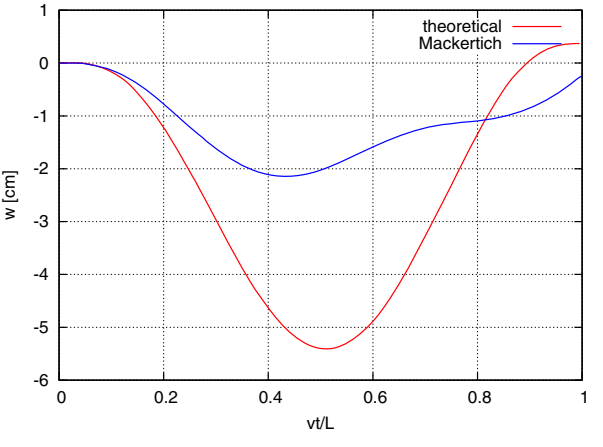

Fig. 4.12 Comparison of results given in [95] with semi-analytical results at the speed v = 50 m/s.

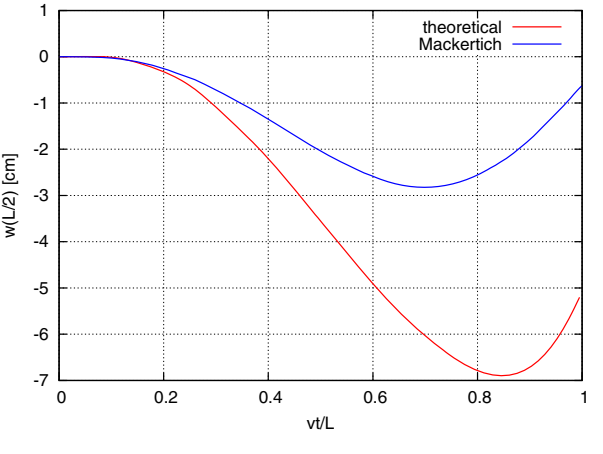

Fig. 4.13 Comparison of results given in [95] with semi-analytical results at the speed v = 100 m/s.

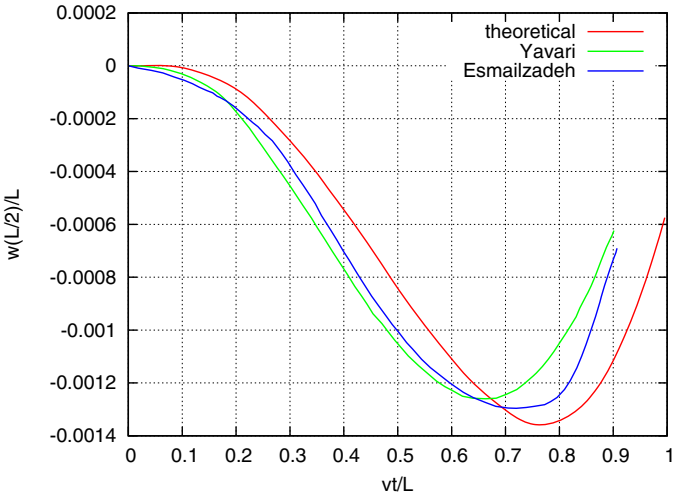

Fig. 4.14 Deflection in the middle of the beam [148] compared with semi-analytical results — rigid beam.

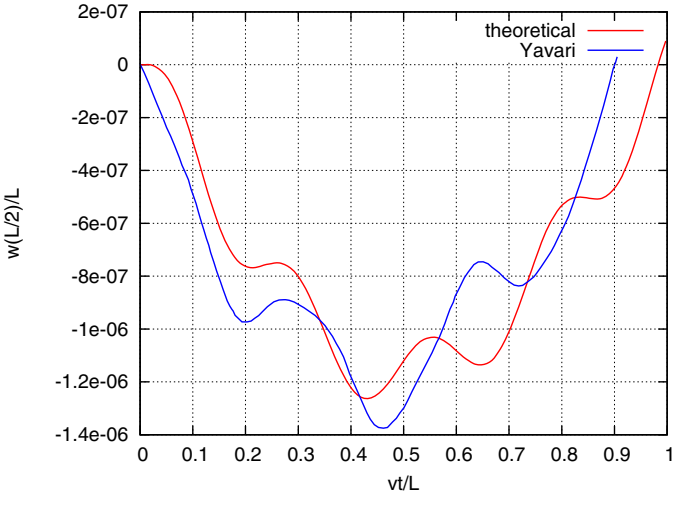

Fig. 4.15 Deflection in the middle of the beam [148] compared with semi-analytical results — soft beam.

100 m/s. The shear wave speed was $c_1 = 2200$ m/s and the bending wave speed was $c_2 = 3740$ m/s. All three Figures 4.11, 4.12, and 4.13 exhibit significant underestimation of the displacements in comparison with the semi-analytical results. The amplitudes were underestimated by more than a factor of two.

Yavari, Noufi, and Mofid in 2002 [148] solved the problem with a discrete method. They called the method the discrete element technique. The continuous

flexible beam elements were replaced by a system of rigid bars and flexible joints. The authors compared their results with those obtained by Esmailzadeh and Gorashi [50]. We compare the displacements in the middle of the span with the theoretical, semi-analytical results. The following data were assumed: $l = 435.2$ cm, $\rho = 15.267$ g/cm^3, $E = 2.02 \cdot 10^{11}$ Pa, $G = 0.77 \cdot 10^{11}$ Pa, $A = 13.1$ cm^2, $I = 57.1$ cm^4,

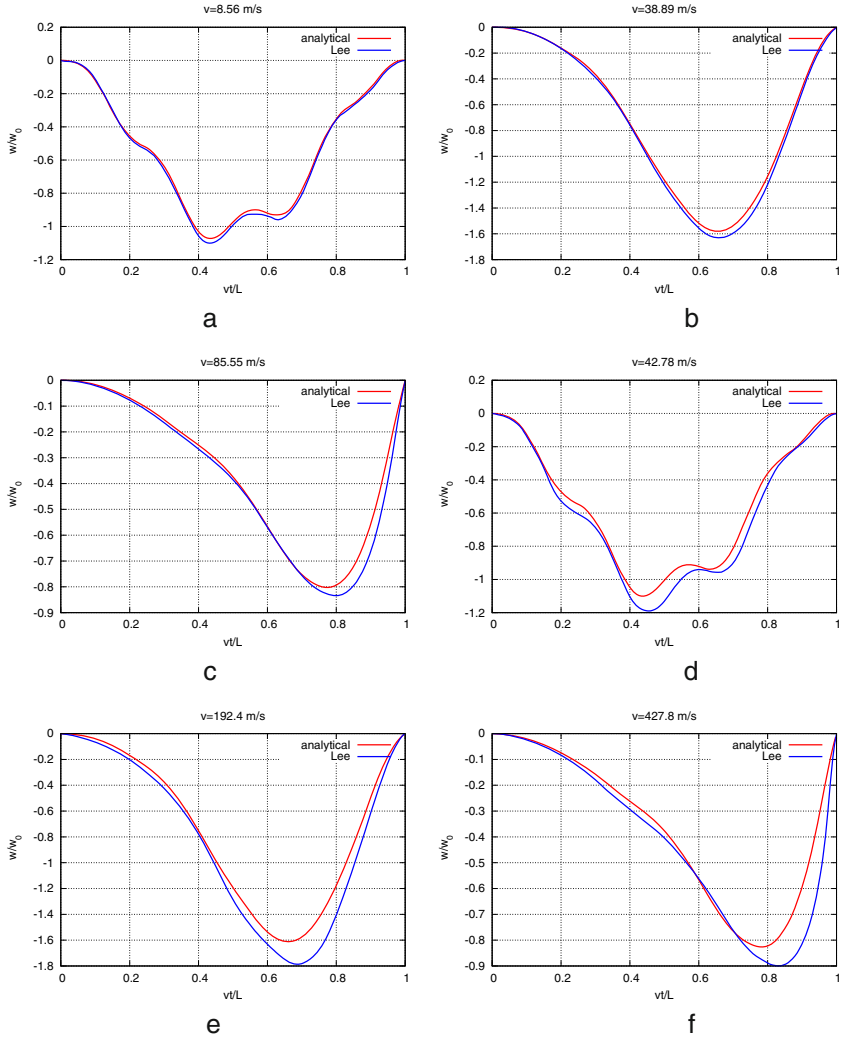

Fig. 4.16 Displacements under a moving mass: a) – $A = 2.865$ cm^2, $I = 0.653$ cm^4, v = 8.56 m/s, b) – $A = 2.865$ cm^2, $I = 0.653$ cm^4, v = 38.89 m/s, c) – $A = 2.865$ cm^2, $I = 0.653$ cm^4, v = 85.55 m/s, d) – $A = 71.62$ cm^2, $I = 408.18$ cm^4, v = 42.78 m/s, e) – $A = 71.62$ cm^2, $I = 408.18$ cm^4, v = 192.4 m/s, f) – $A = 71.62$ cm^2, $I = 408.18$ cm^4, v = 427.8 m/s.

and the shape factor $k = 1.43$. The mass of the span was $M = 87.04$ kg and the moving mass was $m_0 = 21.83$ kg. The speed of the motion was $\mathsf{v} = 27.49$ m/s. We can also give the shearing and bending wave speed: $c_1 = 1878$ m/s, $c_2 = 3637$ m/s. In Figure 4.14, we compare the results from the literature. We notice that the moving mass is relatively small and the speed v, related to the wave speed, is low. In such a case the influence of the moving mass on the beam dynamics is slight. Even in this case, both results are underestimated in comparison to the semi-analytical results. These last we assume to be accurate.

The second example presented in the same paper was computed for the following data: $l = 435.2$ cm, $\rho = 0.0988$ g/cm^3, $E = 2.02 \cdot 10^{11}$ Pa, $G = 0.77 \cdot 10^{11}$ Pa, $A = 2025$ cm^2, $I = 3.42 \cdot 10^5$ cm^4, and the shape factor $k = 1.18$. The mass of the span was $M = 200$ kg and the moving mass was $m_0 = 87.04$ kg. The speed of the motion was $\mathsf{v} = 50$ m/s. The shearing and bending wave speeds are equal to, respectively, c_1=2570 m/s and $c_2 = 4522$ m/s. In Figure 4.15, the mid-span displacements are depicted and compared with the semi-analytical results. Notice that although the maximum amplitude does not differ significantly, the shapes of the curves do not fit.

Lee in [86] expressed the bending and shear energy as a sine and cosine series. The Lagrangian formulation was used. He applied the following data to his examples: $l = 1$ m, $E = 2.07 \cdot 10^{11}$ Pa, $G = 0.776 \cdot 10^{11}$ Pa, and the shape factor $k = 1.11$. The mass density of the span was $\rho = 7700$ kg/m^3. In the first three tests (Figure 4.16a, b, c) the cross sectional area was $A = 2.865$ cm^2 and the cross sectional inertia moment was $I = 0.653$ cm^4. The velocity was increased in each of the three cases and was equal to 8.56, 38.89, and 85.55 m/s, respectively.

Next tests were performed for the following data: $A = 71.62$ cm^2 and $I = 408.18$ cm^4. The velocities were, respectively, 42.78, 192.4, and 427.8 m/s. The moving mass was 0.2 of the mass of the beam in each case. The results are presented in Figure 4.16d, e, f.